This paper describes objective technical results and analysis. Any subjective views or opinions that might be expressed in the paper do not necessarily represent the views of the U.S. Department of Energy or the United States Government.

SAND2020-4057J

Determination of background doping type in type-II superlattice using capacitance-voltage measurements with double mesa structure

D. R. Fink[a], S. Lee[a], S. H. Kodati[a], V. Rogers[a], T. J. Ronningen[a], M. Winslow[b], C. H. Grein[b], A. H. Jones[c], J. C. Campbell[c], J. F. Klem[d], and S. Krishna[a*]

[a] Department of Electrical and Computer Engineering, The Ohio State University, Columbus, Ohio, 43210, USA; [b] Department of Physics, University of Illinois, Chicago, Illinois, 60607, USA; [c] Department of Electrical and Computer Engineering, University of Virginia, Charlottesville, Virginia, 22904, USA; [d] Sandia National Laboratories, Albuquerque, New Mexico 87185, USA
* Krishna.53@osu.edu

ABSTRACT

We present a method of determining the background doping type in semiconductors using capacitance-voltage measurements on overetched double mesa p-i-n or n-i-p structures. Unlike Hall measurements, this method is not limited by the conductivity of the substrate. By measuring the capacitance of devices with varying top and bottom mesa sizes, we were able to conclusively determine which mesa contained the p-n junction, revealing the polarity of the intrinsic layer. This method, when demonstrated on GaSb p-i-n and n-i-p structures, determined that the material is residually doped p-type, which is well established by other sources. The method was then applied on a 10 monolayer InAs/10 monolayer AlSb superlattice, for which the doping polarity was unknown, and indicated that this material is also p-type.

Keywords: Semiconductors, superlattices, doping polarity, capacitance-voltage profiling, double mesa

1. INTRODUCTION

The background doping concentration of unintentionally doped material in p-i-n devices has a large impact on device performance. Since it is affected by temperature, defects, impurities, and their activation energies, it is generally dependent on the material and growth process. While it has been thoroughly studied for many bulk materials, the background doping polarity is not known for many superlattices (SLs) due to their multiple constituents with different background concentrations. For example, type-II superlattices (T2SL) using the antimonide family of semiconductors (InAs, GaSb, AlSb) have established themselves as a promising candidate for infrared (IR) detectors and focal plane arrays[1]. However, their background doping polarity depends on the composition of the layers, their thicknesses, and even temperature[2]. Accurate knowledge of the background doping polarity and magnitude is required to correctly model the device measurements[3,4].

While typical capacitance-voltage (C-V) measurements can determine the magnitude of the background doping concentration in a p-i-n device, they cannot determine the polarity. Some work suggests the sign of dC/dV can be used to determine the polarity[5], but this method is only capable of determining whether the structure is p-i-n or n-i-p. Hall measurements are commonly used to determine the background doping polarity[6], but are limited by parallel conduction in the substrate, and thus cannot be used for materials grown on conductive substrates such as GaSb[7,8]. Various mobility spectrum analyses use Hall measurements as a function of magnetic field to extract information about multiple carriers[9,10,11,12] and have been used to determine carrier polarity in materials, even on some conductive substrates[8]. However, there are challenges to identifying all present carriers using this method – fitting is needed to extract the concentration and mobility values[13], and some carriers may not be visible in the conductivity spectra at all temperatures[14].

To avoid difficulties with conductive substrates, materials can be grown on semi-insulating substrates such as GaAs[15] or with an insulating buffer layer between the material and the conductive substrate[16] to allow Hall measurements and polarity determination. However, both methods could introduce defects that would not be present in material grown directly on the

Sandia National Laboratories is a multimission laboratory managed and operated by National Technology & Engineering Solutions of Sandia, LLC, a wholly owned subsidiary of Honeywell International Inc., for the U.S. Department of Energy's National Nuclear Security Administration under contract DE-NA0003525.

primary substrate, causing measurements from these variant growths to be inapplicable to the actual devices[3,7]. Additionally, the conductivity of a buffer such as AlGaAsSb is dependent on temperature, so this buffer may not be effectively insulating when not at cryogenic temperatures[8]. Since the background doping concentration and polarity can depend on temperature[2], tests limited by temperature are undesirable.

Electrochemical capacitance-voltage (ECV) measurements can be used to determine both the doping concentration and polarity of a material, but there are situations in which this solution would not be preferred. The first is if the device is to be used in future tests, as ECV involves etching a hole through the device[17]. Second, the applied AC signal frequency in ECV setups is typically limited to tens of kHz to reduce the effects of the electrolyte's series resistance[18]. These relatively low frequencies, compared to the MHz used in other C-V measurements, can be problematic when measuring leaky, or low shunt resistance, devices. This is particularly relevant for low bandgap devices, such as mid-wave and long-wave IR photodiodes.

We designed a technique for determining the background doping polarity in semiconductor materials using an overetched double mesa structure, as shown in Figure 1. Unlike the Hall technique, this procedure is not limited by the conductivity of substrates. The key idea is that the overetched double mesa structure creates two junctions with different areas, only one of which is a p/n junction. The UID layer type determines whether the top or bottom mesa contains the p/n junction. Since the device capacitance scales with the area of this junction, we can use C-V measurements on devices with differing mesa sizes to extract the magnitude and polarity of the background doping concentration. We tested this on a UID GaSb sample and a UID 10×10 InAs/AlSb T2SL at room temperature.

2. THEORY

This polarity determination technique is based on two principles. The first is that the diode capacitance is proportional to the p/n junction area.

$$Capacitance = \frac{\varepsilon \cdot area}{d} = \frac{\varepsilon \cdot \pi \cdot radius^2}{d}$$

The second is that the effective capacitance of a p/n junction in series with the n^-/n^+ or p^-/p^+ junction, as in a p-i-n device, is dominated by the p/n junction. This is because the impedance of series-connected elements is dominated by the element of highest impedance. By design, the n^-/n^+ and p^-/p^+ junction has a low impedance, while the p/n junction has a high impedance that is primarily capacitive. In other words, we can assume for this analysis that the impedance of the n^-/n^+ or p^-/p^+ junction does not affect the capacitance measurements.

To implement the technique, p-i-n devices are made with a double mesa architecture. Depending on the polarity of the UID layer, the p/n junction is either located at the top contact/UID interface or at the UID/bottom contact interface. For instance, for a p-i-n (p on n) device and a p-type UID layer, the p/n junction will be at the UID/bottom contact (i-n, p^-/n^+) interface. Thus, the capacitance will vary with the bottom mesa radius and be independent of the top mesa radius (neglecting the capacitance of the top p^+/p^- junction). Similarly, if the same p-type UID layer is in a n-i-p (n on p) architecture, then the p/n junction will be at the top contact/UID (n-i, n^+/p^-) interface, the capacitance will vary with the top mesa radius, and the capacitance will be independent of the bottom mesa radius (neglecting the capacitance of the bottom p^-/p^+ junction).

This concept is illustrated through a simulation of the electric field in p-i-n and n-i-p diodes made with GaSb as shown in Figure 1. GaSb is known to be a residually p-type material[7,15] due to the high number of Ga_{Sb} antisite defects[17]. In diodes, the electric field is highest within the depletion region at the p/n junction. In the simulated p-i-n structure, the field is highest within the bottom mesa, and in a n-i-p structure, the field is highest within the top mesa.

The expected capacitance vs. radius data for the p-i-n and n-i-p GaSb structures simulated above is shown graphically in Figure 2(a). Figure 2(b) shows theoretical data for a structure of residually n-type material with otherwise equivalent structural and material properties. Depending on the residual doping type, capacitance should have no relationship with the chosen mesa (top or bottom) area for one structure but should scale linearly with area (quadratically with radius) in the other. Capacitance arising from surface effects would manifest as a mostly linear increase with radius, making surface effects separable from mesa area effects. While the polarity of the material can be concluded from a single growth (either p-i-n or n-i-p), both are shown below.

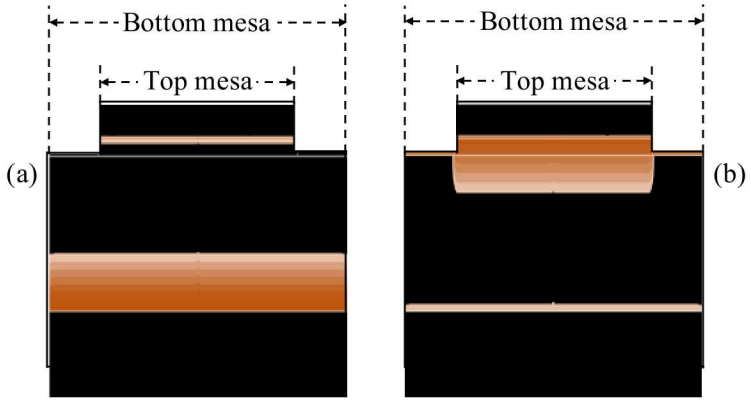

Figure 1: Simulation results for electric field in GaSb p-i-n (a) and n-i-p (b) devices. The area and location of the high electric field (dark regions) depends on the mesa in which the p/n junction is contained.

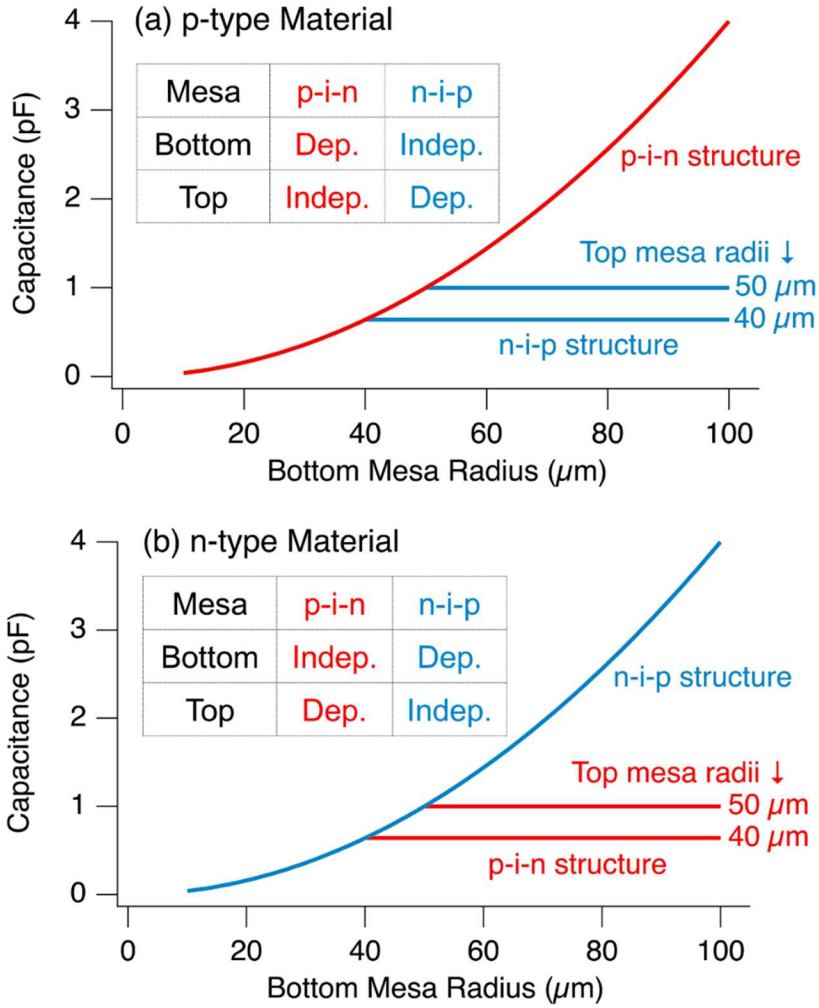

Figure 2: Theoretical capacitance vs. bottom mesa radius plots for fully depleted p-i-n and n-i-p structures, comparing results for (a) p-type and (b) n-type materials. For each structure, capacitance is dependent on one mesa size and independent of the other. Note that the top mesa radius cannot exceed the bottom mesa radius, limiting the data range.

3. GROWTH AND FABRICATION

Photodiodes are commonly used and studied today due to their applications in imaging, communications, LIDAR, sensing, and more. IR photodiodes are commonly used for environmental sensing (due to molecular signatures in the IR), telecommunications (due to low losses or dispersion[19]), and thermal imaging (due to the thermal emission of heat sources in the mid-wave and long-wave IR). Superlattices are a developing technology that provide the potential for band structure engineering due to their many structural variables. Photodiodes are commonly grown in a p-i-n structure, as the extended length and low doping of the intrinsic layer increases device absorption.

Two sets of samples were grown to study material characteristics for photodetector applications. The first set was of p-i-n and n-i-p GaSb structures, grown on n-GaSb substrates by solid source molecular beam epitaxy (SSMBE). This material is of interest due to a previous study showing that GaSb has very high quantum efficiency in the near-infrared (NIR)[20], making it attractive for potential telecommunications applications. A 1000 nm UID GaSb layer was grown between the 200 nm top contact and 500 nm bottom contact layers. Both contact layers were doped at 2×10^{18} cm^{-3}.

The second set was of p-i-n and n-i-p 10×10 InAs/AlSb SL structures, grown on n-GaSb substrates by SSMBE. Band structure simulations indicated that this material could impact ionize and create gain with relatively low excess noise while detecting NIR light. These characteristics would make this material excellent for APDs. A 1000 nm UID SL layer was grown between 300 and 500 nm top and bottom contacts, respectively. Both contact layers were doped at 2×10^{18} cm^{-3}. A UID GaSb buffer layer was grown between the bottom contact and the substrate.

All four samples were fabricated into double mesa devices. Top and bottom contacts were formed by Ti (20 nm)/Au (200 nm) deposition by e-beam evaporator. A dry etch recipe involving BCl_3 and Ar was used for the formation of shallow and deep mesas. For p-i-n devices, the average shallow and deep mesa depths were 340 nm and 1210 nm from the top, respectively. For n-i-p devices, the average shallow and deep mesa depths were 285 nm and 1264 nm from the top, respectively. The devices were SU-8 passivated. Table I outlines the mesa radii of the fabricated and tested devices.

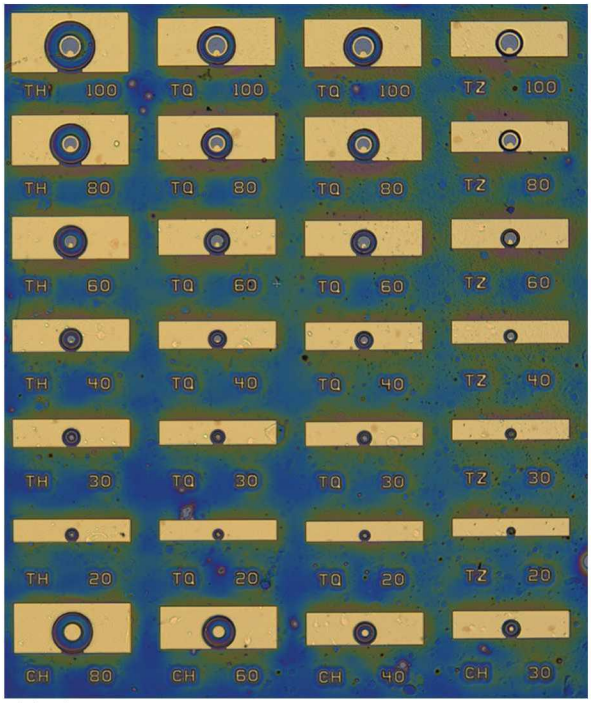

Figure 3: Picture of the fabricated device array.

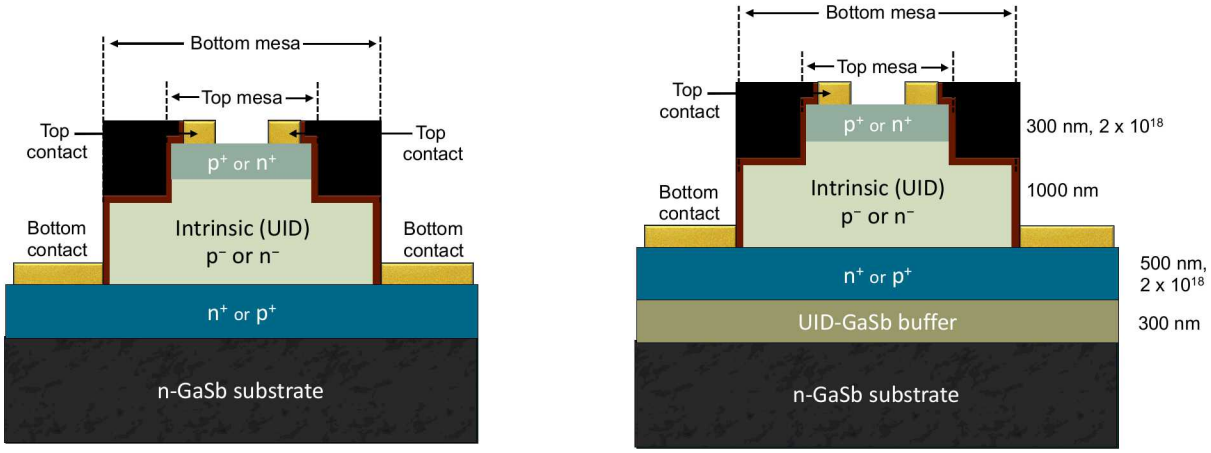

Figure 4: Schematics of the GaSb devices (left) and the InAs/AlSb SL devices (right).

Table I. Combinations of top and bottom mesa radii for fabricated devices. Data were analyzed only if, for a given structure and top mesa radius, all three devices were functional.

Top mesa radius	Bottom mesa radius	Analyzed For
20 µm	20 µm 30 µm 40 µm	GaSb p-i-n
30 µm	30 µm 45 µm 60 µm	GaSb p-i-n
40 µm	40 µm 60 µm 80 µm	GaSb n-i-p, InAs/AlSb p-i-n, InAs/AlSb n-i-p
50 µm	50 µm 75 µm 100 µm	GaSb n-i-p, InAs/AlSb p-i-n, InAs/AlSb n-i-p

4. RESULTS

4.1 GaSb

The GaSb samples described previously were brought to vacuum and measured at 295 K. Test setup parameters were chosen to maximize the quality factor (Q), the ratio of the measured reactance and resistance[5]. A moderate magnitude of 50 mV was chosen for the applied AC signal and yielded sufficiently low noise (<5 fF RMS). The measurement frequency was chosen to be 1 MHz, yielding maximum quality factors over 25 and almost 10 for the InAs/AlSb p-i-n and n-i-p samples, respectively. The voltage was swept from 1 V to -10 V with a hold (or integration) time of 500 ms and a delay time (time between measurements) of 100 ms. Data from the six GaSb p-i-n devices listed in Table I are reported below.

From this data, the depletion width and background doping concentration were calculated[18], arbitrarily choosing the top mesa area of the device as the p/n junction area. Loess (Locally Estimated Scatterplot Smoothing) regression[21] was

implemented in MATLAB to smooth the calculated background doping concentration. A span of 8% was used for the Loess algorithm.

The surface leakage in the diodes was large and degraded the measurement accuracy. A threshold of $Q \geq 3$ to accept the data was chosen, which translates to a maximum error in the measured capacitance of 9%[5]. This is sufficient for the purpose of determining the background doping polarity. The quality factor starts to diminish around -6 V, and falls below 3 slightly beyond -8 V, as shown in Figure 5. The plot of doping vs depletion width is shown in Figure 6 for biases up until this point.

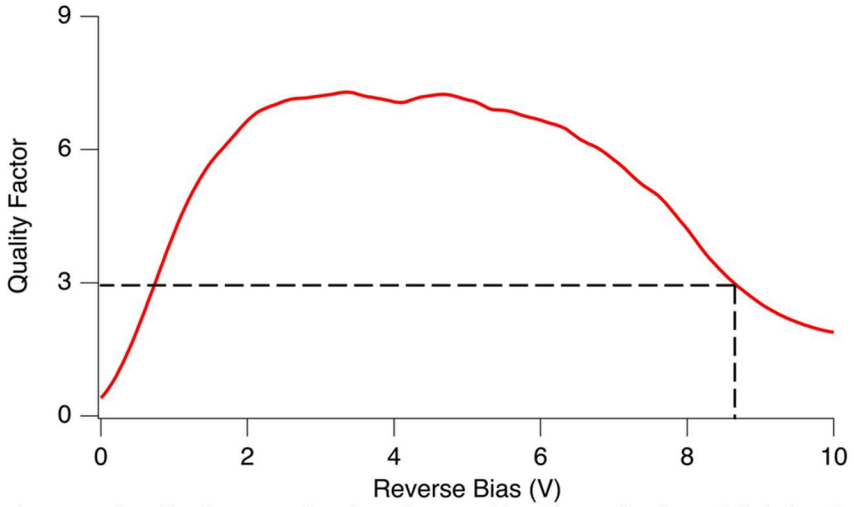

Figure 5: A sample curve of quality factor as a function of reverse bias. The quality factor falls below 3 slightly beyond an 8 V reverse bias.

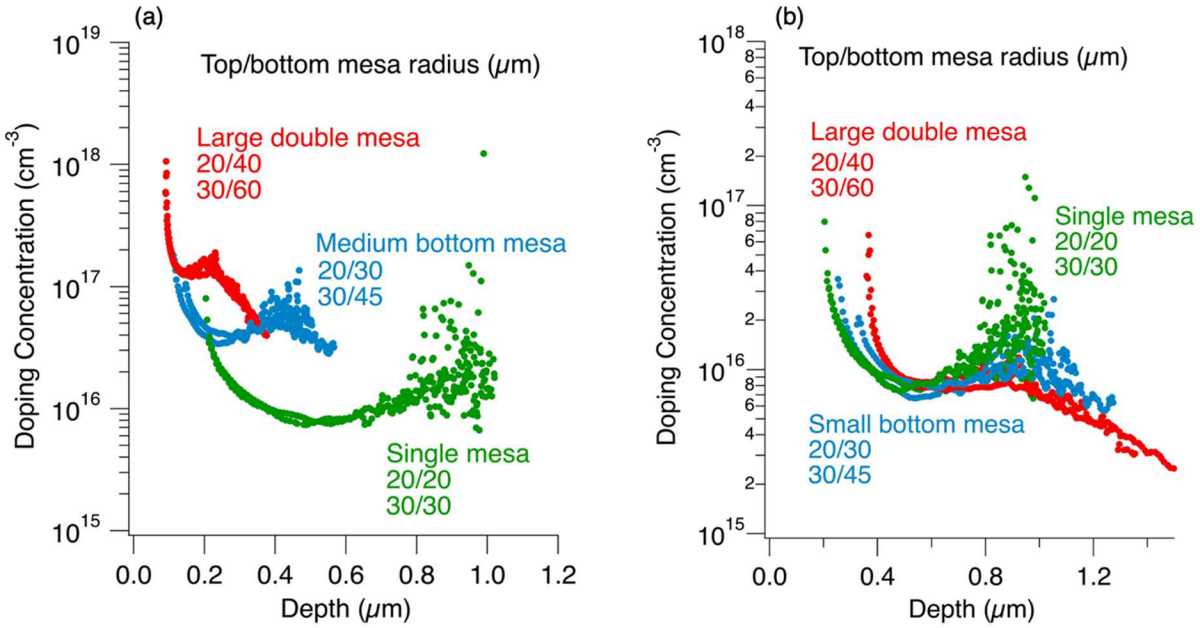

Figure 6: Loess-smoothed doping concentration as a function of depletion width for the GaSb p-i-n devices using (a) the top mesa area as the active area (b) the bottom mesa area as the active area.

Figure 6(a) shows an odd trend – the calculated doping concentration differs from device to device, which should not be the case for devices on the same sample. However, devices with the same bottom mesa radius factor (1×, 1.5×, or 2× the top mesa radius) seem to be grouped together. To try to find an explanation for this, the data is reanalyzed assuming the p/n junction is in the bottom mesa, which changes the relevant areas in the calculations (see Figure 6(b)). The calculated

doping concentration now makes more sense, as all six devices are all approximately 8×10^{15} cm^{-3}, particularly in regions where the data is least noisy. This suggests that *the p/n junction is in the bottom mesa for the p-i-n devices and indicates the UID layer is p-type.*

For the n-i-p devices, the devices were swept from -1 V to 3 V. In these devices the conductance started higher and increased sooner than for the p-i-n devices, yielding a very limited range of accurate data. During analysis of this data the top mesa was assumed to contain the p/n junction, which would be accurate if the UID layer is p-type. In the very small region over which the quality factor is greater than 3, the background doping concentration is approximately 1.3×10^{16} cm^{-3}. The location of the p/n junction provides a possible explanation of the difference in quality factors between the two structures – because the junction was buried in the bottom mesa for the p-i-n devices, surface effects did not have as large an impact on the conductivity.

Next, the same capacitance data was plotted as a function of device radius to try to identify the background doping polarity. Data from both p-i-n and n-i-p structures are shown in Figure 7 for a -0.7 V bias, as the leakiness of the n-i-p devices rapidly degraded the measurement quality at higher voltages. The devices were not fully depleted at this bias.

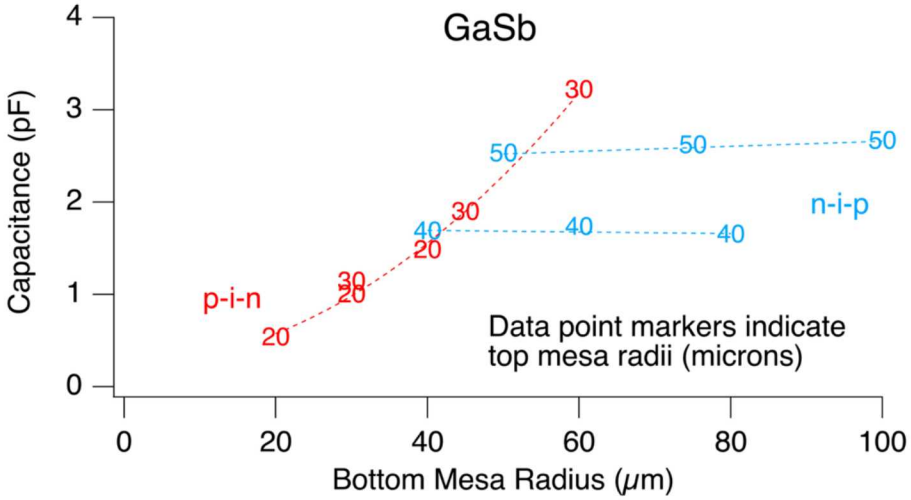

Figure 7: GaSb p-i-n and n-i-p results with fitted curves. These graphs show that the capacitance is dependent on bottom mesa radius for the p-i-n structures, and the top mesa radius for the n-i-p structures. This indicates the material is p-type.

For the p-i-n GaSb devices, the capacitance scales quadratically with bottom mesa radius, but shows no dependence on top mesa radius, indicating that the p/n junction is in the bottom mesa. The n-i-p devices show no dependence with bottom mesa radius, but increases with top mesa radius, indicating that the p/n junction is in the top mesa. Both show that for GaSb, the measured capacitance is dependent on the area between the n-type and UID layers, as shown in Figure 8. *This determines that the material is p-type,* as expected.

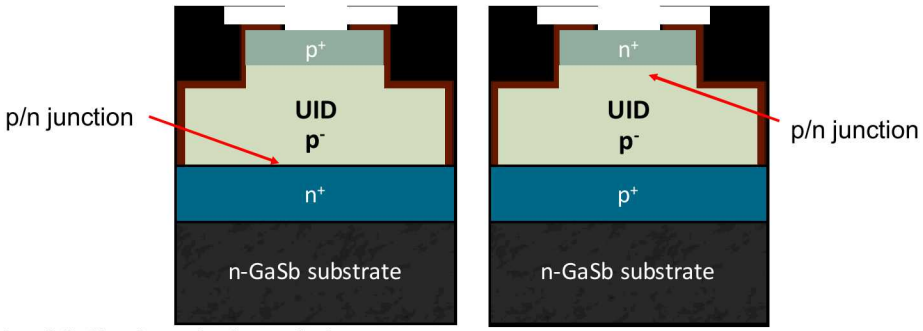

Figure 8: Results of GaSb p-i-n and n-i-p analysis.

The measured capacitance is higher than the theoretical results shown in Figure 2 because the devices were not fully depleted, reducing the equivalent parallel plate separation distance.

In summary, two slightly different methods have been used to determine the background doping polarity in GaSb devices, both using C-V measurements of multiple double mesa devices with varying mesa sizes to find the location of the p/n junction. The first determines which mesa area used in the background doping concentration calculations results in matching concentrations for each device. The second plots capacitance vs radius and determines which mesa area is related to the device capacitance, as described previously in this manuscript. While both methods are based on the same principles, the second method is preferred due to the ease of computation and analysis.

4.2 10×10 InAs/AlSb

The 10×10 InAs/AlSb SL samples were tested as well. The same test conditions were used as with the GaSb devices. As for the previous set of samples, the background doping concentration was calculated by first arbitrarily assuming that the p/n junction is contained in the top mesa. The plot of doping vs. depletion width is shown in Figure 9(a) for biases between -6 and 0 V, the region where the quality factor is greater than 3.

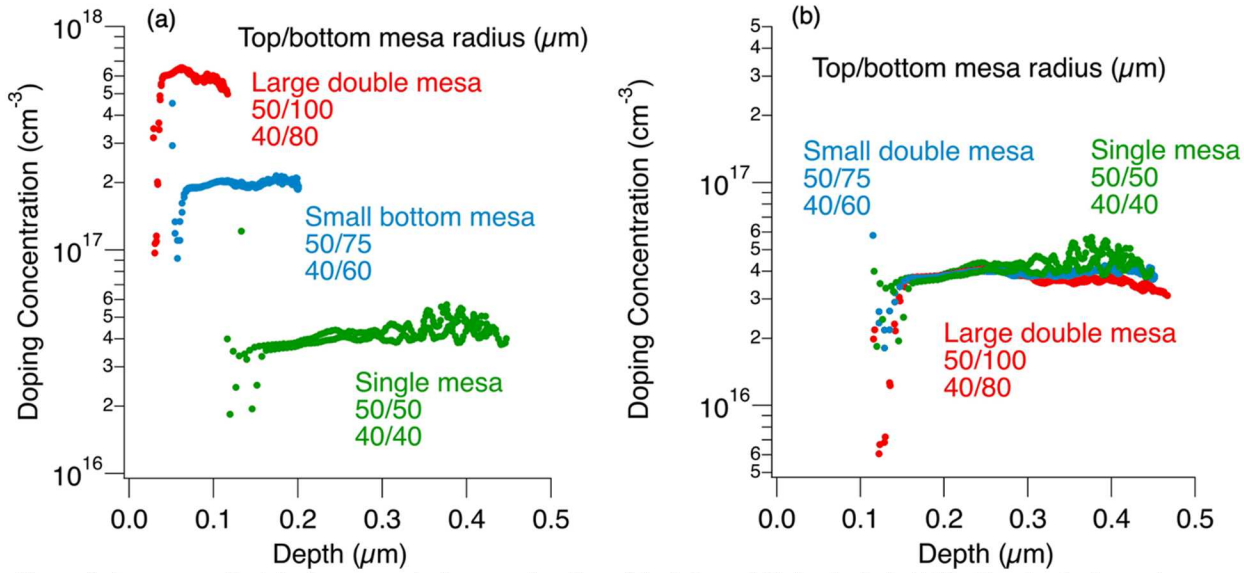

Figure 9: Loess-smoothed doping concentration as a function of depletion width for the InAs/AlSb SL p-i-n devices using (a) the top mesa area as the active area (b) the top mesa area as the active area..

Again, the data seems to indicate that the devices have different background doping concentrations, but devices with the same bottom mesa radius factor are grouped together. The analyses are repeated, this time assuming the p/n junction is contained in the bottom mesa (see Figure 9(b)). Once again, the results with the new assumption that the bottom mesa area is the active area make much more sense. This suggests that *the p/n junction is in the bottom mesa, and thus the is material is p-type.* The background doping concentration is very similar for all devices, at approximately 3.8×10^{16} cm^{-3}.

This same process is applied for the SL n-i-p devices (see Figure 10(a)). Since the p-i-n results suggested the UID layer might be p-type, it was first assumed that the p/n junction might be in the top mesa for the n-i-p devices. The large double mesa devices had a significantly lower quality factor than the single mesa devices and a slightly higher quality factor than the small double mesa devices. The doping concentration was plotted for the full bias range for the single mesa devices, and at biases between 0 and 4 V for the others.

The doping concentrations for these devices surprisingly do not all match. The calculated doping concentrations of the large double mesa and single devices are approximately 6×10^{15} cm^{-3}, but almost double that for the small double mesa devices. The analyses were repeated using the bottom mesa area as the active area to see if this condition creates a better match (see Figure 10(b)). Clearly, with this assumption, the mismatch is even greater. The high calculated background doping concentration of the two small bottom mesa devices is perhaps related to the difference in quality factors. The lower the quality factor, the greater the potential error, and the small double mesa devices have the lowest quality factors of the set. The reason for the difference in quality factors in this case is unknown.

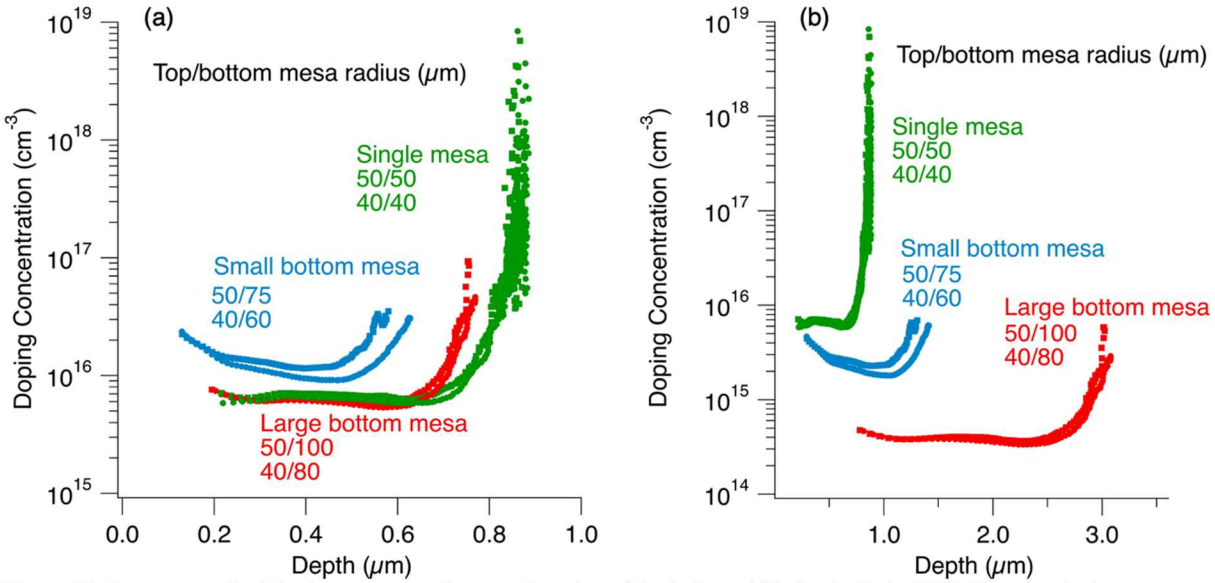

Figure 10: Loess-smoothed doping concentration as a function of depletion width for the InAs/AlSb SL n-i-p devices assuming (a) the top mesa area is the active area (b) the bottom mesa area is the active area.

The background doping polarity determination method was applied to both the p-i-n and n-i-p samples. The unintentional doping polarity of this material was not known, for while InAs is n-type[7,15,22] and AlSb is p-type[23], it was unclear which dominates in 10×10 SL material[15,16]. A bias of 3 V was chosen for comparison. This higher bias was possible because the devices were less leaky than the GaSb devices and had higher quality factors. Any voltage between 0 and 3 V would also have been a legitimate choice. The results for this material are shown in Figure 11.

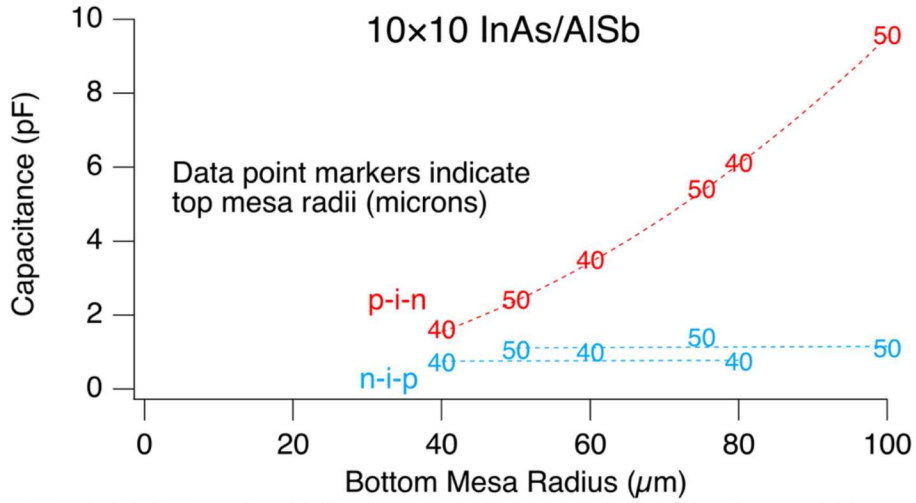

Figure 11: 10×10 InAs/AlSb SL results with fitted curves. Both structures indicate that the material is p-type.

For the p-i-n devices, the capacitance scales quadratically with bottom mesa radius, but shows no dependence on top mesa radius, indicating that the p/n junction is in the bottom mesa. The n-i-p devices show no dependence with bottom mesa radius, but increases with top mesa radius, indicating that the p/n junction is in the top mesa. Both show that the measured capacitance is dependent on the area between the n-type and UID layers. This result determines that 10×10 InAs/AlSb UID material is p-type, and the p-type AlSb dominates over the n-type InAs. Due to their lower background doping concentration, the n-i-p devices depleted more quickly than the p-i-n devices, explaining why the n-i-p capacitance is lower than the p-i-n capacitance. While it has been shown that temperature can flip the polarity in superlattices[2], preliminary results on the InAs/AlSb SL n-i-p devices show that the material is still p-type at 8 K and 77 K.

5. Conclusions

In conclusion, a method for determining the background doping polarity of semiconductor layers has been established. This method is not limited by temperature or substrate conductivity and does not destroy the devices under test. This method was verified by measuring p-i-n and n-i-p GaSb devices and determined that this material is residually p-type, which was previously known. This method was also applied to p-i-n and n-i-p 10×10 InAs/AlSb devices and established that his material is also residually p-type, which was previously unknown. Though the polarities of UID bulk materials are commonly known, the vast variability of SL materials provides usage cases for this method.

ACKNOWLEDGEMENTS

This work is supported by the Directed Energy–Joint Transition Office, Award N00014-17-1-2440. This work was performed, in part, at the Center for Integrated Nanotechnologies, an Office of Science User Facility operated for the U.S. Department of Energy (DOE) Office of Science. Sandia National Laboratories is a multimission laboratory managed and operated by National Technology & Engineering Solutions of Sandia, LLC, a wholly owned subsidiary of Honeywell International, Inc., for the U.S. DOE's National Nuclear Security Administration under contract DE-NA-0003525. This paper describes objective technical results and analysis. Any subjective views or opinions that might be expressed in the paper do not necessarily represent the views of the U.S. Department of Energy or the United States Government. D. F. wishes to thank Hyemin Jung for assistance with Figure 4 and Figure 8.

REFERENCES

[1] A. Rogalski, P. Martyniuk, and M. Kopytko, "Type-II superlattice photodetectors versus HgCdTe photodiodes," Prog. Quant. Electron., 68, 100228-100247 (2019).

[2] C. Cervera, J. B. Rodriguez, J. P. Perez *et al.*, "Unambiguous determination of carrier concentration and mobility for InAs/GaSb superlattice photodiode optimization," J. Appl. Phys., 106(3), 033709-033712 (2009).

[3] A. Hood, D. Hoffman, Y. Wei *et al.*, "Capacitance-voltage investigation of high-purity InAs/GaSb superlattice photodiodes," Appl. Phys. Lett., 88(5), 052112-052114 (2006).

[4] C. Anayama, T. Tanahashi, H. Kuwatsuka *et al.*, "High□purity GaSb epitaxial layers grown from Sb□rich solutions," Appl. Phys. Lett., 56(3), 239-240 (1990).

[5] O. Bierwagen, T. Nagata, T. Ive *et al.*, "Dissipation-factor-based criterion for the validity of carrier-type identification by capacitance-voltage measurements," Appl. Phys. Lett., 94, 152110-152112 (2009).

[6] T. Asar, S. Özçelik, and E. Özbay, "Structural and electrical characterizations of InxGa1-xAs/InP structures for infrared photodetector applications," J. Appl. Phys., 115(10), 104502-104508 (2014).

[7] H. J. Haugan, S. Elhamri, G. J. Brown *et al.*, "Growth optimization for low residual carriers in undoped midinfrared InAs/GaSb superlattices," J. Appl. Phys., 104(7), 073111-073114 (2008).

[8] T. V. Chandrasekhar Rao, J. Antoszewski, L. Faraone *et al.*, "Characterization of carriers in GaSb/InAs superlattice grown on conductive GaSb substrate," Appl. Phys. Lett., 92(1), 012121-012123 (2008).

[9] W. A. Beck, and J. R. Anderson, "Determination of electrical transport properties using a novel magnetic field□dependent Hall technique," J. Appl. Phys., 62(2), 541-554 (1987).

[10] J. R. Meyer, C. A. Hoffman, J. Antoszewski *et al.*, "Quantitative mobility spectrum analysis of multicarrier conduction in semiconductors," J. Appl. Phys., 81(2), 709-713 (1997).

[11] I. Vurgaftman, J. R. Meyer, C. A. Hoffman *et al.*, "Improved quantitative mobility spectrum analysis for Hall characterization," J. Appl. Phys., 84(9), 4966-4973 (1998).

[12] D. Chrastina, J. P. Hague, and D. R. Leadley, "Application of Bryan's algorithm to the mobility spectrum analysis of semiconductor devices," J. Appl. Phys., 94(10), 6583-6590 (2003).

[13] T. V. Chandrasekhar Rao, J. Antoszewski, J. B. Rodriguez *et al.*, "Quantitative mobility spectrum analysis of carriers in GaSb/InAs/GaSb superlattice," J. Vac. Sci. Technol. B, 26(3), 1081-1083 (2008).

[14] G. A. Umana-Membreno, B. Klein, H. Kala *et al.*, "Vertical minority carrier electron transport in p-type InAs/GaSb type-II superlattices," Appl. Phys. Lett., 101(25), 253515-253518 (2012).

[15] A. Khoshakhlagh, F. Jaeckel, C. Hains *et al.*, "Background carrier concentration in midwave and longwave InAs/GaSb type II superlattices on GaAs substrate," Appl. Phys. Lett., 97(5), 051109-051111 (2010).

[16] L. Bürkle, F. Fuchs, J. Schmitz *et al.*, "Control of the residual doping of InAs/(GaIn)Sb infrared superlattices," Appl. Phys. Lett., 77(11), 1659-1661 (2000).
[17] J. Shen, H. Goronkin, J. D. Dow *et al.*, "Explanation of the origin of electrons in the unintentionally doped InAs/AlSb system," J. Vac. Sci. Technol. B, 13(4), 1736-1739 (1995).
[18] D. K. Schroder, [Semiconductor Material and Device Characterization] John Wiley & Sons, Inc., Hoboken, NJ (2006).
[19] L. A. Coldren, S. W. Corzine, and M. L. Masanovic, [Diode Lasers and Photonic Integrated Circuits] John Wiley and Sons, Hoboken, New Jersey (2012).
[20] F. Capasso, M. B. Panish, and P. W. Foy, "Very high quantum efficiency GaSb mesa photodetectors between 1.3 and 1.6 μm," Appl. Phys. Lett., 36, 165-167 (1980).
[21] R. A. Irizarry, [Introduction to Data Science] CRC Press, (2020).
[22] C. Yi, T. Kim, and A. S. Brown, "InAs-Based p-n Homojunction Diodes: Doping Effects and Impact of Doping on Device Parameters," J. Electron. Mater., 35(9), 1712-1714 (2005).
[23] C. A. Chang, H. Takaoka, L. L. Chang *et al.*, "Molecular beam epitaxy of AlSb," Appl. Phys. Lett., 40(11), 983-985 (1982).